Constraint effects on probabilistic analysis of cracks in ductile solids

S. RAHMAN and G. CHEN

Department of Mechanical Engineering, The University of Iowa, Iowa City, IA 52242, USA

Received in final form 14 March 2000

ABSTRACT This paper presents a method for evaluating constraint effects on probabilistic elastic–plastic analysis of cracks in ductile solids. It is based on fracture parameters $\mathcal{J}$ and Q, correlation between Q and $\mathcal{J}$–resistance curve of the material, and $\mathcal{J}$-tearing theory for predicting fracture initiation and instability in cracked structures. Based on experimental data from small-scale fracture specimens, correlation equations were developed for fracture toughness at crack initiation and the slope of the $\mathcal{J}$–resistance curve as a function of constraint condition. The random parameters may involve crack geometry, tensile and fracture toughness properties of the material, and applied loads. Standard reliability methods were applied to predict probabilistic fracture response and reliability of cracked structures. The results suggest that crack-tip constraints have little effect on the probability of crack initiation. However, the probability of fracture instability can be significantly reduced when constraint effects are taken into account. Hence, for a structure where some amount of stable crack-growth can be tolerated, crack-tip constraints should be considered for probabilistic fracture-mechanics analysis.

Keywords crack; crack-tip constraint; elastic–plastic fracture mechanics; probabilistic fracture mechanics; $\mathcal{J}$-integral; Q parameter; $\mathcal{J}$–resistance curve; $\mathcal{J}$–Q analysis; single-edged-notched bend specimens.

NOMENCLATURE

a = crack size; crack depth of single-edged-notched bend specimen
B = thickness of single-edged-notched bend specimen
$C(Q)$ = constraint-based slope of $\mathcal{J}$–resistance curve
$\tilde{C}(Q)$ = normalized slope of $\mathcal{J}$–resistance curve
$D_{ij}, E_{ij}, F_{ij}, G_{ij}, H_{ij}$ = constant coefficients
$\boldsymbol{D}, \boldsymbol{E}, \boldsymbol{F}, \boldsymbol{G}, \boldsymbol{H}$ = matrices involving coefficients, $D_{ij}, E_{ij}, F_{ij}, G_{ij}, H_{ij}$
E = Young's modulus
$f_{\boldsymbol{X}}(\boldsymbol{x})$ = joint probability density function of $\boldsymbol{X}$
h_1 = dimensionless plastic influence function
$\mathcal{J}$ = $\mathcal{J}$-integral
$\mathcal{J}_{\mathrm{e}}$ = elastic component of $\mathcal{J}$
$\mathcal{J}_{\mathrm{p}}$ = plastic component of $\mathcal{J}$
$\mathcal{J}_R(\Delta a)$ = $\mathcal{J}$-resistance curve
$\mathcal{J}_R(\Delta a, Q)$ = constraint-dependent $\mathcal{J}$–resistance curve
$\mathcal{J}_{\mathrm{Ic}}(Q)$ = constraint-based mode-I plane-strain fracture toughness at initiation
$\tilde{\mathcal{J}}_{\mathrm{Ic}}(Q)$ = normalized mode-I plane-strain fracture toughness at initiation
$\mathcal{J}(\boldsymbol{X})$ = $\mathcal{J}$-integral as a function of random vector, $\boldsymbol{X}$
k_{init} = probability ratio for fracture initiation
k_{ins} = probability ratio for fracture instability
K_{I} = mode-I stress-intensity factor
n = Ramberg–Osgood exponent
n_j = jth component of unit outward normal to integration path, $\mathrm{d}\Gamma$
N = number of input random variables
P = load; load on single-edged-notched bend specimen

Correspondence: S. Rahman. E-mail: rahman@icaen.uiowa.edu

P_i = initiation load
P_{init} = probability of fracture initiation
P_{ins} = probability of fracture instability
P_{max} = maximum load
P_0 = reference load
Pr = probability operator
Q = constraint parameter
$Q(\boldsymbol{X})$ = constraint parameter as a function of random vector, $\boldsymbol{X}$
r, θ = polar coordinates
S = span of single-edged-notched bend specimen
T_i = ith component of traction vector
$u_{i,1}$ = derivative of displacement, u_i with respect to x_1
W = width of single-edged-notched bend specimen
$\boldsymbol{x}$ = realization of $\boldsymbol{X}$
$\boldsymbol{X}$ = an N-dimensional random vector
α = Ramberg–Osgood coefficient
Γ = counterclockwise contour
δ_{ij} = Kronecker delta
Δa = extension of crack length
ε = uniaxial strain
ε_0 = reference strain
ν = Poisson's ratio
σ = uniaxial stress
σ_{ij} = stress field
$\sigma_{ij,SSY}$ = reference stress field (small-scale yielding solution)
σ_0 = reference stress
$\sigma_{\theta\theta,SSY}$ = circumferential reference stress (small-scale yielding solution)
$\sigma_{\theta\theta}$ = circumferential stress
$\mathscr{E}$ = expectation (mean) operator
$\mathscr{W}$ = strain energy density
$\cap$ = intersection of two events

INTRODUCTION

Current elastic–plastic fracture-mechanics analysis of cracks typically involves fracture toughness properties of materials measured using high-constraint specimen geometries, e.g. deeply cracked three-point bend specimens. Questions arise if the fracture toughness curves, e.g. $\mathcal{J}$–resistance ($\mathcal{J}$–R) curves, measured from these specimens can be applied to structural applications with low-constraint crack geometries (Fig. 1). A reverse problem occurs when the fracture toughness data are obtained on relatively low-constraint specimens and then used in high-constraint applications. In this case, the material $\mathcal{J}$–R curve is obtained from a specimen of standard thickness (e.g. 25 mm or lower), but the application is much larger, e.g. a reactor pressure vessel with thickness well over 200 mm. Hence, both conservative and non-conservative predictions of fracture behaviour and reliability can occur even if stringent ASTM requirements are met for calculating $\mathcal{J}$–R curves of a material. This raises a fundamental question on how to incorporate constraint effects on fracture-mechanics evaluation of cracked structures.

It is now well known in the fracture-mechanics community that a single fracture parameter, e.g. the $\mathcal{J}$-integral, alone may not be adequate to describe crack-tip conditions under general large-scale yielding in solids.[1] To address this problem, there has been a recent surge of interest in crack-growth behaviour under conditions of low crack-tip stress triaxiality. A primary impetus to this activity has been a set of efforts aimed at developing two-parameter descriptions of crack-tip fields. Retaining consistency with traditional approaches, the first parameter reflects the scale of crack-tip deformation (e.g. $\mathcal{J}$). A second parameter is used to identify a particular member of a family of crack-tip fields of varying stress triaxiality. There are several approaches to this second parameter characterization. Of these, the characterizations based on the normalized T-stress[2,3] and on the local triaxiality perturbation (Q)[4,5] appear to be promising for the evaluation of constraint effects on

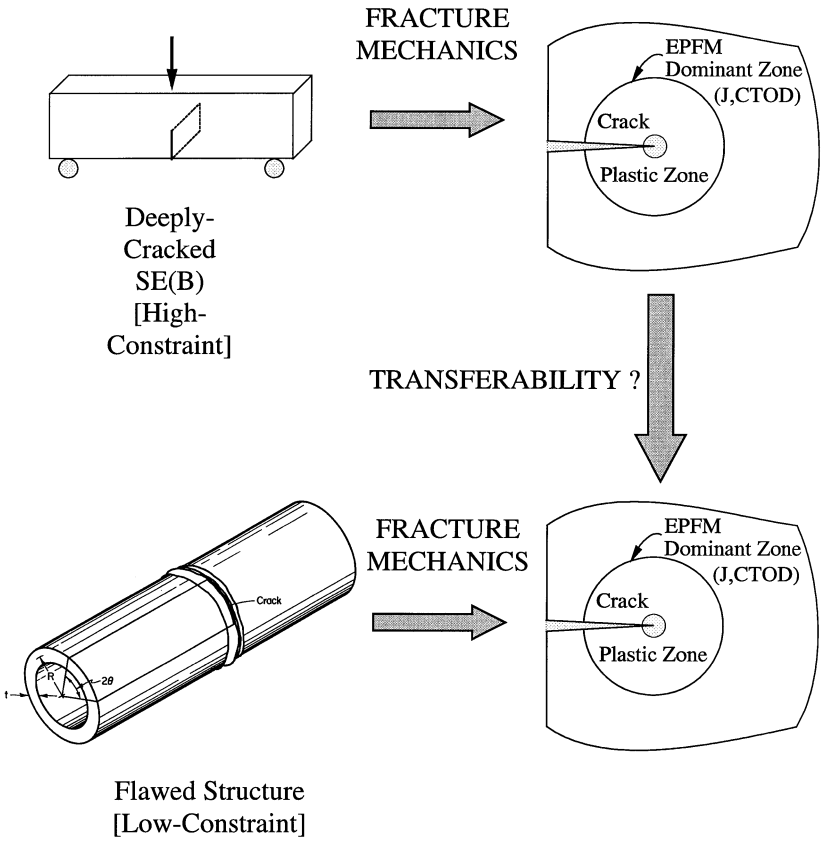

Fig. 1 Transferability of fracture toughness data from small-scale specimens.

material toughness. An excellent review comparing several features of both T-stress and Q-formalisms has been performed by Parks.[3] Although these two approaches and parameters have much in common, there are differences which can have significant practical implications.[3] Under well-contained yielding, the T-stress is appropriate and is a much simpler constraint theory to apply compared with the Q-formalism. Actually, under such conditions, these two approaches and parameters are uniquely related. However, for large-scale plasticity, the T-stress approach, which is based on surrounding elastic singularity, becomes invalid. In such a case, the constraint theory based on Q is more appropriate than T-stress. This is a major reason why constraint evaluation based on the Q parameter has received far more attention than that based on T-stress.

Most (if not all) constraint evaluations performed to date are purely deterministic. This gives an incomplete picture of the constraint effects on fracture due to uncertainties in loads, material properties and crack size. Probabilistic fracture mechanics, which blends the probability theory with the principles of fracture mechanics, provides a more realistic evaluation of cracked structures. While development is still ongoing, probabilistic fracture models, based on elastic–plastic analysis and J-integral-based ductile tearing theory, have appeared already. For example, a stochastic model, based on an engineering approximation of the J-integral and first- and second-order reliability methods (FORM/SORM), has been developed by Rahman[6,7] for fracture analysis of cracked tubular structures. Based on this model, the probability of crack-growth initiation and subsequent fracture instability under quasi-static external loads can be predicted. This model has been subsequently enhanced by a more general model[8,9] in which the values of the J-integral needed by FORM/SORM are calculated by elastic–plastic finite element analysis. However, all existing models are based on the single J-integral fracture parameter. Hence, there is a clear need to develop probabilistic methods that can account for constraint effects on fracture. To the best knowledge of the authors, no such methods or studies exist in the current literature. This is the major motivation for the present study described in this paper.

This paper presents a probabilistic methodology to account for constraint effects on fracture in ductile solids. The methodology involves: (i) elastic–plastic fracture mechanics for calculating fracture parameters, J and Q; (ii) correlation between fracture toughness properties of the material and constraint parameter, Q; and (iii) J-tearing theory for predicting fracture initiation and instability in cracked structures. The random param-

eters involve crack geometry, tensile and fracture toughness properties of the material, and applied loads. Standard reliability methods were applied to predict the probabilistic fracture response and reliability of cracked structures.

J–Q ANALYSIS

Consider a two-dimensional cracked body in a state of plane-strain condition. Assume that the constitutive law characterizing the material's stress–strain (σ–ε) response can be represented by the well-known Ramberg–Osgood model, which is given by

$$\frac{\varepsilon}{\varepsilon_0} = \frac{\sigma}{\sigma_0} + \alpha\left(\frac{\sigma}{\sigma_0}\right)^n \tag{1}$$

where σ_0 is the reference stress which is usually assumed to be the yield stress, E is the modulus of elasticity, $\varepsilon_0 = \sigma_0/E$ is the associated reference strain, and α and n are the model parameters usually chosen from best fit of actual laboratory data. For an arbitrary counterclockwise path, Γ around the crack tip, a formal definition of $\mathcal{J}$ under mode-I condition is:[10–12]

$$\mathcal{J} \overset{\text{def}}{=} \int_\Gamma (\mathcal{W} n_1 - T_i u_{i,1})\, \mathrm{d}\Gamma \tag{2}$$

where, $\mathcal{W}$ is the strain energy density, u_i and T_i are the ith component of displacement and traction vectors, respectively, n_j is the jth component of unit outward normal to integration path, $\mathrm{d}\Gamma$ is the differential length along contour Γ, and $u_{i,1}$ is the differentiation of displacement, u_i with respect to x_1. For this material, the stress state in the vicinity ($r \to 0$) of a stationary crack tip can be expressed by:[4,5]

$$\sigma_{ij}(r, \theta) = \sigma_{ij,\mathrm{SSY}}(r, \theta) + Q\sigma_0\delta_{ij} \tag{3}$$

where r and θ are polar coordinates with their origin at the crack tip, $\sigma_{ij}(r, \theta)$ is the stress field, $\sigma_{ij,\mathrm{SSY}}(r, \theta)$ is the reference stress field representing small-scale yielding solution and thus directly connected to $\mathcal{J}$, δ_{ij} is the Kronecker delta, and Q is a constraint parameter quantifying the deviation in hydrostatic stress from the small-scale yielding solution, scaled by σ_0. By setting $\theta = 0$ in Eq. (3) and examining the $\sigma_{\theta\theta}$ stress component, Q can be defined as

$$Q = \frac{\sigma_{\theta\theta}(r, 0) - \sigma_{\theta\theta,\mathrm{SSY}}(r, 0)}{\sigma_0} \tag{4}$$

Because the non-singular term is not constant but rather a slowly varying field, Eq. (4) needs to be applied for a specific value of r. In this study, it was assumed that $r = 2\mathcal{J}/\sigma_0$. Given a cracked body with known load, material and geometry, the fracture parameters, $\mathcal{J}$ and Q, can be calculated by the finite element method using Eqs (2) and (4), respectively.

THE *J*–RESISTANCE CURVE

If $\mathcal{J}$ is a valid fracture parameter, the fracture resistance of a material can be described by the $\mathcal{J}$–resistance curve, $\mathcal{J}_R(\Delta a)$, where the fracture toughness, $\mathcal{J}_R$, depends on the crack extension, Δa, but not on the absolute crack length. However, for large-scale yielding in finite bodies, the relationship between $\mathcal{J}$ and near-tip fields loses uniqueness. This lack of uniqueness, often termed as loss of constraint, increases the fracture toughness of the material observed for many tension and bend specimens. Indeed, the mismatch of constraint conditions at the crack tip plays a significant role on the transferability (or lack thereof) of fracture behaviour of small-scale fracture specimens to the behaviour of large-scale structures.[1]

However, with the introduction of Q as a constraint parameter, one can correlate Q with the $\mathcal{J}$–resistance curve of the material. For example, assume that the $\mathcal{J}$–R curve can be modelled by a linear equation, given by

$$\mathcal{J}_R(\Delta a, Q) = \mathcal{J}_{\mathrm{Ic}}(Q) + C(Q)\Delta a \tag{5}$$

where $\mathcal{J}_{\mathrm{Ic}}(Q)$ is mode-I plane-strain fracture toughness at crack initiation and $C(Q)$ is the slope of the $\mathcal{J}$–R curve, both of which depend on Q. By varying Q in small-scale fracture specimens, $\mathcal{J}_{\mathrm{Ic}}(Q)$ and $C(Q)$ can be easily estimated for a given material and temperature. Figure 2 shows schematically how Q affects the $\mathcal{J}$–R curve of a material.

For convenience, define two normalized fracture toughness parameters, as follows

$$\tilde{\mathcal{J}}_{\mathrm{Ic}}(Q) = \frac{\mathcal{J}_{\mathrm{Ic}}(Q)}{\mathcal{J}_{\mathrm{Ic}}(0)} \tag{6}$$

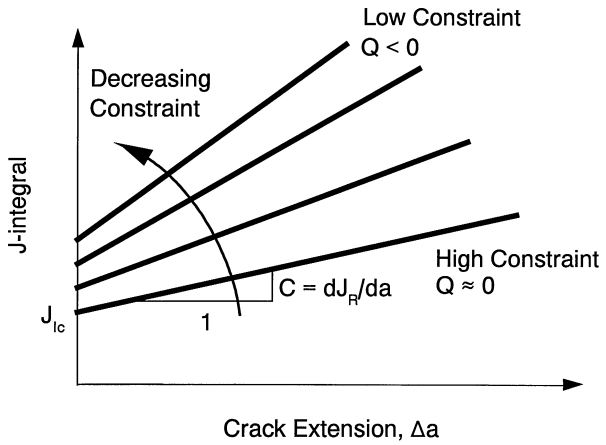

Fig. 2 Effects of Q on fracture toughness curve of a material.

and

$$\tilde{C}(Q) = \frac{C(Q)}{C(0)} \tag{7}$$

which represent the ratios of constraint-dependent fracture toughness parameters to their high-constraint values. Using Eqs (6) and (7), one can now estimate the $\mathcal{J}$–R curve of a material for any constraint condition, provided the expressions for $\tilde{\mathcal{J}}_{\mathrm{Ic}}(Q)$ and $\tilde{C}(Q)$ and their high-constraint ($Q = 0$) values are known.

PROBABILISTIC FRACTURE MECHANICS

$\mathcal{J}$–Q-based failure criteria

For any monotonically loaded cracked structure, regardless of geometry, equal values of $\mathcal{J}$ and Q mean equal crack-tip conditions. Thus, the philosophy of using $\mathcal{J}$ and Q to characterize initiation and instability of crack growth may be mathematically stated as[13]

$$\text{Crack initiation:} \quad \mathcal{J} = \mathcal{J}_{\mathrm{Ic}}(Q) \tag{8}$$

$$\text{Crack instability:} \quad \begin{cases} \mathcal{J} = \mathcal{J}_R(\Delta a, Q) \\ \dfrac{\partial \mathcal{J}}{\partial a} = \dfrac{\mathrm{d}\mathcal{J}_R}{\mathrm{d}a}(\Delta a, Q) \end{cases} \tag{9}$$

respectively. The left sides of Eqs (8) and (9) represent the crack driving force and its rate, while $\mathcal{J}_{\mathrm{Ic}}(Q)$ and $\mathcal{J}_R(\Delta a,Q)$, representing fracture toughness at crack initiation and at crack growth, Δa, respectively, are the constraint-dependent crack resistance properties of the material. If one can calculate $\mathcal{J}$ and Q for a given structure, fracture initiation and instability can be predicted from the constraint-dependent $\mathcal{J}$–R curve of the material.

The initiation of crack growth in a structure containing flaws can be characterized when the crack-driving force ($\mathcal{J}$) exceeds the material fracture toughness ($\mathcal{J}_{\mathrm{Ic}}$). Equation (8) represents this failure criterion. This is a good definition of failure when the uncracked ligament is small (e.g. part-through surface cracks in pipes or through-wall cracks in small-diameter pipes) or the amount of subsequent stable crack growth is limited (e.g. cracks in brittle materials). The initiation-based failure criterion is commonly used in piping and pressure vessel analysis.[14]

In elastic–plastic fracture mechanics theory, the stable crack growth, if it occurs in a structure, can also be characterized by the $\mathcal{J}$-integral parameter with some limitations. In this regard, the $\mathcal{J}$-tearing theory is a very prominent concept to quantify the stable crack growth. It is based on the fact that fracture instability can occur after some amount of stable crack growth in tough and ductile materials with an attendant higher applied load level at fracture. The onset of fracture instability is defined when $\mathcal{J}$ and $\partial\mathcal{J}/\partial a$ exceed $\mathcal{J}_R$ and $\mathrm{d}\mathcal{J}_R/\mathrm{d}a$ simultaneously, as also expressed by Eq. (9). The corresponding crack-instability load is either equal to or higher than the crack-initiation load. The difference between these two failure loads can be significant, if the structural geometry and material permit appreciable amount of stable crack growth. Otherwise, the fracture criterion based on the initiation of crack growth provides a conservative estimate of structural integrity. Figure 3 summarizes the fracture assessment procedure using the $\mathcal{J}$–Q-based fracture criteria described in this paper.

Random parameters and fracture response

Consider a cracked structure with uncertain mechanical and geometric characteristics that is subject to random loads. Denote by $\boldsymbol{X}$ an N-dimensional random vector with components $X_1, X_2, \ldots, X_N$ characterizing all uncertainty in the system and load parameters. Let $\mathcal{J}(\boldsymbol{X})$ and $Q(\boldsymbol{X})$ be two relevant fracture response parameters that can be calculated from elastic–plastic finite element analysis. Suppose that the structure fails when the crack-driving force exceeds the fracture resistance of the material. For example, consider the failure criterion: $\mathcal{J}(\boldsymbol{X}) > \mathcal{J}_{\mathrm{Ic}}(Q)$. This requirement cannot be satisfied with certainty, because both $\mathcal{J}$ and Q depend on input vector $\boldsymbol{X}$ which is random, and $\mathcal{J}_{\mathrm{Ic}}(Q)$ itself is a random variable. Hence, the performance of the cracked structure should be evaluated by the associated probability of failure, P_{F}. More specifically, consider the failure probability, P_{init}, which represents the probability of initiation of crack growth [see Eq. (8)]. Mathematically,

$$P_{\mathrm{init}} \overset{\mathrm{def}}{=} \Pr[\mathcal{J}(\boldsymbol{X}) > \mathcal{J}_{\mathrm{Ic}}(Q)] = \int_{\mathcal{J}(\boldsymbol{x}) > \mathcal{J}_{\mathrm{Ic}}} f_{\boldsymbol{X}}(\boldsymbol{x})\, \mathrm{d}\boldsymbol{x} \tag{10}$$

where $f_{\boldsymbol{X}}(\boldsymbol{x})$ is the joint probability density function of $\boldsymbol{X}$. For more realistic performance evaluation, consider another failure probability, P_{ins}, representing the probability of crack instability [see Eq. (9)]. Mathematically, it can be defined as

$$\begin{aligned} P_{\mathrm{ins}} &\overset{\mathrm{def}}{=} \Pr\left[\{\mathcal{J}(\boldsymbol{X}) > \mathcal{J}_R(\Delta a, Q)\} \cap \left\{\frac{\partial \mathcal{J}(\boldsymbol{X})}{\partial a} > \frac{\mathrm{d}\mathcal{J}_R}{\mathrm{d}a}(\Delta a, Q)\right\}\right] \\ &= \Pr\left[\{\mathcal{J}(\boldsymbol{X}) > \mathcal{J}_R(\Delta a, Q)\} \,\middle|\, \left\{\frac{\partial \mathcal{J}(\boldsymbol{X})}{\partial a} > \frac{\mathrm{d}\mathcal{J}_R}{\mathrm{d}a}(\Delta a, Q)\right\}\right] \\ &\quad \times \Pr\left[\frac{\partial \mathcal{J}(\boldsymbol{X})}{\partial a} > \frac{\mathrm{d}\mathcal{J}_R}{\mathrm{d}a}(\Delta a, Q)\right] \end{aligned} \tag{11}$$

As mentioned before, Eq. (10) represents the probability of initiation of crack growth, which provides a conserva-

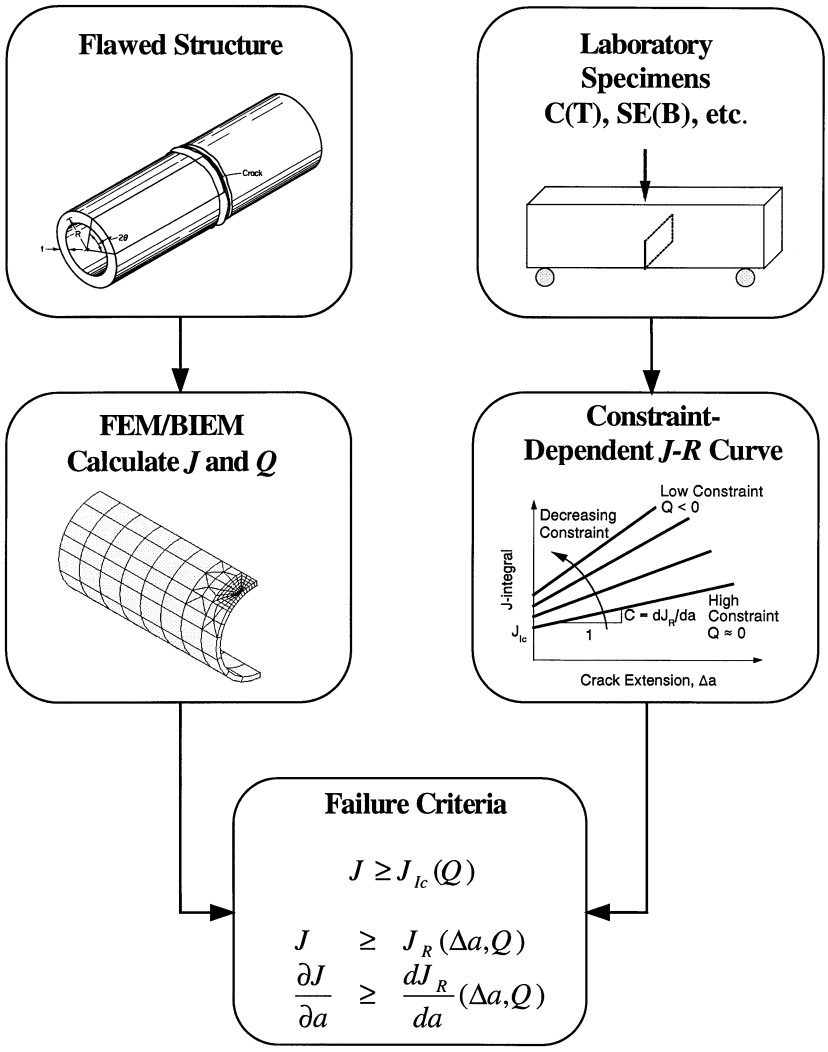

Fig. 3 Fracture assessment based on $\mathcal{J}$–Q analysis.

tive estimate of structural performance. A less conservative evaluation requires calculation of failure probability based on crack-instability criterion. The latter probability, shown in Eq. (11), is more difficult to compute because it must be obtained by incorporating crack-growth simulation in a non-linear finite element analysis. However, if suitable approximations of $\mathcal{J}$ can be developed analytically, it can be easily calculated as well.[6,7]

Structural reliability analysis

The generic expression for the probabilities in Eqs (10) and (11) involves multidimensional probability integration for their evaluations. This is explicitly shown in Eq. (10). Similar integral expressions can also be developed for both probabilities on the right-hand side of Eq. (11). Standard reliability methods, e.g. FORM/SORM,[15–18] and Monte Carlo simulation,[19] can be used to compute these multidimensional integrals, and hence, the failure probabilities. In FORM/SORM, the failure probabilities are calculated based on linear and quadratic approximations, respectively, of the performance (limit-state) function at the design point (also known as most probable point, beta point, etc.). The determination of the design point involves non-linear constrained optimization and is performed in the standard Gaussian image of the original space. The Monte Carlo simulation involves repeated deterministic evaluations of the performance function due to independently generated realizations of random input. Details of FORM/SORM and simulation are readily available in the current literature.[15–19] They are not described here for brevity. It is worthwhile to note that these methods have been successfully applied to probabilistic fracture-mechanics analysis of cracked structures based on the single $\mathcal{J}$-integral fracture parameter. See past work of Rahman and others[6–9] for further details.

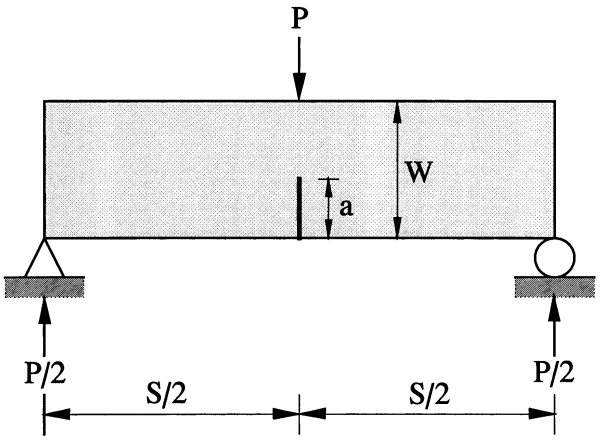

Fig. 4 Single-edge-notched bend specimen.

APPLICATIONS

The single-edge-notched bend structure

Consider a two-dimensional cracked structure subjected to three-point bend loads as shown in Fig. 4. The material is HY80 steel. The load, P, crack depth, a, width, W, thickness, B and bend span, S are shown. Assume that the plane-strain condition exists for this structure. The objective of this example is to demonstrate how constraint affects the failure probability of this cracked structure. In this study, all probabilistic calculations were performed based on the second-order reliability method.

Constraint-dependent $\mathcal{J}$–R curve

Recently, Joyce and Link[20] developed experimental data on quasi-static fracture toughness properties of HY80 steel at room temperature. The tests were performed using 1T single-edge-notched bend [SE(B)] specimens according to ASTM E1737-96.[21] A total of 14 specimens were loaded in three-point bending with a bend span of 203 mm, a span-to-width (S/W) ratio of 4, and a thickness-to-width (B/W) ratio of 0.5. The crack depth-to-width ratio (a/W) varied from 0.13 to 0.83 to simulate various constraint conditions. The measured values of $\mathcal{J}_{Ic}$ and C varied from 145.6 to 225.6 kJ/m^2 and 80 768 to 172 403 kJ/m^3, respectively. Correspondingly, Q varied from -0.1 to -0.7 at the crack-driving force of $\mathcal{J}_{Ic}$. Table 1 shows the values of $\mathcal{J}_{Ic}$, C and Q for various a/W, obtained by Joyce and Link.[20] Using the data in Table 1, Fig. 5 shows the plots of measured $\tilde{\mathcal{J}}_{Ic}(Q)$ and $\tilde{C}(Q)$ for various values of Q. Following linear regression analysis by least-squares, $\tilde{\mathcal{J}}_{Ic}(Q)$ and $\tilde{C}(Q)$ can be expressed by

$$\tilde{\mathcal{J}}_{Ic}(Q) = 1 - 0.307Q \tag{12}$$

Table 1 Fracture toughness for various crack-tip constraints[20]

a/W	$\mathcal{J}_{Ic}$, kJ/m^2	C, kJ/m^3	Q^*
0.29	211.8	140 683	−0.36
0.26	225.6	145 529	−0.43
0.19	217.2	152 725	−0.60
0.39	216.0	114 397	−0.24
0.55	195.2	105 880	−0.15
0.55	169.2	104 411	−0.10
0.13	219.3	160 655	−0.70
0.14	215.1	172 403	−0.70
0.14	183.0	146 851	−0.67
0.13	196.5	159 627	−0.68
0.61	189.5	80 768	−0.10
0.83	162.9	108 229	−0.25
0.78	145.6	115 572	−0.22
0.70	172.6	82 383	−0.15

*Q was calculated at $\mathcal{J} = \mathcal{J}_{Ic}$.

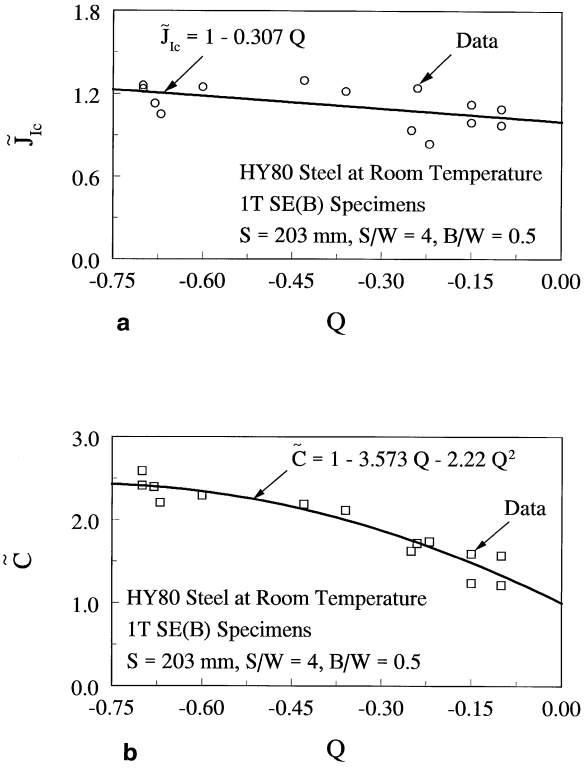

Fig. 5 Non-dimensional toughness parameters for various Q: (a) $\tilde{\mathcal{J}}_{Ic}$ versus Q; (b) $\tilde{C}$ versus Q.

and

$$\tilde{C}(Q) = 1 - 3.573Q - 2.22Q^2 \tag{13}$$

Using Eqs (12) and (13), one can now estimate the $\mathcal{J}$–R curve of a material for any constraint condition, provided the high-constraint toughness parameters, $\mathcal{J}_{Ic}(0)$ and $C(0)$, are known.

Table 2 Statistical properties of random input variables

Random variable	Mean	COV*	Probability distribution
Elastic modulus (E)	228.8 GPa	0.05	Gaussian
Ramberg–Osgood coefficient (α)	1	0.15	Lognormal
Ramberg–Osgood exponent (n)	10	0.15	Lognormal
High-constraint initiation toughness [$\mathcal{J}_{Ic}(0)$]	173.86 kJ/m^2	0.2	Lognormal
High-constraint toughness slope [$C(0)$]	66 540 kJ/m^3	0.1	Lognormal
Normalized crack length (a/W)	Variable	0.1	Gaussian
Load (P)	Variable	0.1	Gaussian

*Coefficient of variation (COV) = standard deviation/mean.

Input parameters

For this numerical example, consider the following random parameters: E, α, n, $\mathcal{J}_{Ic}(0)$, $C(0)$, a/W and P. Table 2 shows the means, coefficients of variation, and probability distributions of these parameters. Note, the statistics and distribution properties of the random input were defined quite arbitrarily and were used only to illustrate the numerical example.

For other deterministic input, the following parameters were used: $S = 2.032$ m (80 inches), $W = 0.508$ m (20 inches), $B = 1$ m (39.4 inches), $\sigma_0 = 445.6$ MPa (64 630 psi), and $\nu = 0.3$.

Results and discussion

For the calculation of failure probabilities (probability of crack initiation or instability), the crack-driving forces $\mathcal{J}$ and Q must be calculated for a given structure. In general, one needs to perform elastic–plastic finite element analysis to predict $\mathcal{J}$ and Q. However, for the three-point bend structure considered in this example (see Fig. 4), closed-form solutions of $\mathcal{J}$ and Q can be developed. See Appendices A and B, which describe the procedures for calculating $\mathcal{J}$ and Q, respectively, for SE(B) specimen. Hence, for a SE(B) specimen with known geometry, loads and material properties, the values of $\mathcal{J}$ and Q can be calculated readily.

Because this SE(B) example problem involves only one load parameter, let P_i and P_{max} denote the initiation load (i.e. the load when crack-growth initiates) and maximum load (i.e. the load when crack-growth becomes unstable), respectively. Note, due to uncertain input, both P_i and P_{max} are random variables. Accordingly, Fig. 6(a) and (b) shows the calculated probability density functions of P_i and P_{max}, respectively, for shallow

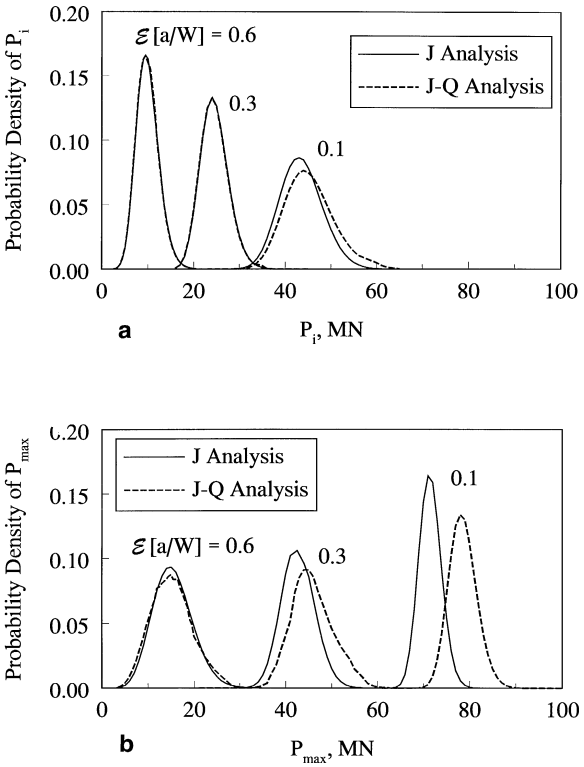

Fig. 6 Effects of Q on probability density of loads: (a) initiation load; (b) maximum load.

($\mathcal{E}[a/W] = 0.1$), intermediate ($\mathcal{E}[a/W] = 0.3$) and deep ($\mathcal{E}[a/W] = 0.6$) cracks considered in this example. Two sets of results—one based on single fracture parameter $\mathcal{J}$ (i.e. ignoring constraint) and the other based on dual fracture parameters, $\mathcal{J}$ and Q (i.e. considering constraint)—are shown in these figures. The following trends can be observed. First, the probability densities of both P_i and P_{max} predicted by $\mathcal{J}$ and $\mathcal{J}$–Q analyses can be different for shallow cracks. This is due to significant loss of constraint for shallow cracks and resultant higher fracture toughness of the material. In Fig. 6(a) and (b), the probability densities from $\mathcal{J}$–Q analysis shift towards the right indicating larger failure loads for shallow and intermediate cracks with low crack-tip constraints. Second, the constraint effects are much smaller on the probability density of P_i than that of P_{max}. This is because of weak dependency of $\mathcal{J}_{Ic}$ on Q, exhibited by Fig. 5(a) or Eq. (12). Deterministic observation consistent with the above probabilistic trend has been reported by some researchers in the past.[1,20] Third, when the crack length increases, the density functions of P_i or P_{max} from $\mathcal{J}$ and $\mathcal{J}$–Q analyses become close to each other. This is due to Q-values approaching zero (high-constraint value) that translates to an insignificant increase in the fracture toughness of the material. Hence, analysis of deep cracks in actual structures can be based

on single fracture parameter (e.g. $\mathcal{J}$) and high-constraint toughness properties of the material.

Perhaps, a more meaningful result is to determine how the constraint affects the probability of failure in a cracked structure for a given applied load. Let $k_{\text{init}} = P_{\text{init}}(Q)/P_{\text{init}}(0)$ and $k_{\text{ins}} = P_{\text{ins}}(Q)/P_{\text{ins}}(0)$ denote two probability ratios, where $P_{\text{init}}(0)$ and $P_{\text{ins}}(0)$ are probabilities of fracture initiation and instability, respectively, from $\mathcal{J}$-analysis, and $P_{\text{init}}(Q)$ and $P_{\text{ins}}(Q)$ are probabilities of fracture initiation and instability, respectively, from $\mathcal{J}$–Q analysis. The ratios, k_{init} and k_{ins}, which depend on crack-tip constraint, can be used to determine if failure probability estimates based on $\mathcal{J}$-integral analysis alone underestimate or overestimate failure probabilities from $\mathcal{J}$–Q analysis. Figure 7(a) and (b) shows the plots of k_{init} and k_{ins}, respectively, as a function of mean applied load, $\mathcal{E}[P]$. As before, three sets of results are presented for various crack lengths ($\mathcal{E}[a/W] = 0.1$, 0.3, and 0.6), and hence, for various magnitudes of constraint. According to Fig. 7(a), no major constraint effects were found on the probability of fracture initiation. For example, when the mean applied load is 20 MN, the probabilities of fracture initiation for the shallow crack ($\mathcal{E}[a/W] = 0.1$) are 2.19×10^{-8} and 1.08×10^{-8} from $\mathcal{J}$ and $\mathcal{J}$–Q analyses, respectively. Correspondingly, $k_{\text{init}} = 0.494$ [see Fig. 7(a)] and hence, the probability of fracture initiation for the shallow crack can be decreased by a factor of only 2.02 ($1/k_{\text{init}}$) for this SE(B) example problem when constraint effects are taken into account. This is not a significantly large number when comparing small failure probabilities described earlier. Furthermore, no major constraint effects were found on the probability of fracture initiation for intermediate and deep cracks as shown in Fig. 7(a).

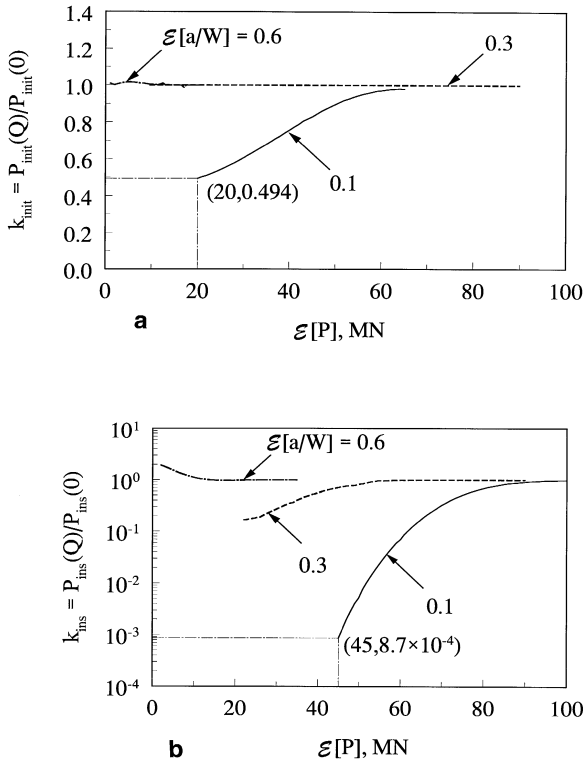

Fig. 7 Probability ratio versus mean applied load: (a) k_{init}; (b) k_{ins}.

However, according to Fig. 7(b), the probability of fracture instability can be significantly decreased by constraint loss in fracture toughness properties, particularly for shallow cracks. This is due to more significant increase in the slope of the $\mathcal{J}$–R curves, shown in Fig. 5(b) or Eq. (13), for low-constraint crack geometries. For example, in Fig. 7(b), when the $\mathcal{E}[P] = 45$ MN, $P_{\text{ins}}(0) = 1.24 \times 10^{-7}$ and $P_{\text{ins}}(Q) = 1.08 \times 10^{-10}$, and hence, $k_{\text{ins}} = 8.7 \times 10^{-4}$ for the shallow crack ($\mathcal{E}[a/W] = 0.1$). Consequently, when constraint effects are taken into account, the probability of fracture instability of SE(B) specimen for the shallow crack can be reduced by a factor of 1149 ($1/k_{\text{ins}}$), which is significantly larger than the factor associated with the probability of fracture initiation. Hence, for a structure where some stable crack growth can be tolerated, crack-tip constraints should be considered for probabilistic fracture-mechanics analysis. However, further studies with more realistic cracked structures and geometry other than that considered in this paper need to be undertaken to make a generic conclusion.

Note, the crack instability criterion used in this paper is based on $\mathcal{J}$–Q theory for stationary crack. Hence, it cannot reflect the increase of crack-tip constraint, if any, due to ductile crack growth. If this constraint is raised significantly, the proposed approach may overestimate the increase of the slope of the fracture–toughness curves. This issue was not explored in the current paper.

CONCLUSIONS

A probabilistic methodology was developed for elastic–plastic fracture-mechanics analysis of cracks in the presence of constraint effects. The methodology involves calculating fracture parameters $\mathcal{J}$ and Q, establishing correlation between constraint parameter Q and fracture toughness properties of the material, and using $\mathcal{J}$-tearing theory for predicting fracture initiation and instability in cracked structures. Based on experimental data from small-scale fracture specimens, correlation equations were developed for fracture toughness at crack initiation and the slope of the $\mathcal{J}$–resistance curve as a function of Q. For probabilistic analysis, the random parameters may involve crack geometry, tensile and fracture toughness properties of the material, and applied loads. Standard reliability methods were applied to predict probabilistic fracture response and reliability of cracked

structures. The results indicate that crack-tip constraint has little effect on the probability of fracture initiation. However, the probability of fracture instability can be significantly reduced when constraint effects are taken into account. Hence, for a structure where some amount of stable crack growth can be tolerated, crack-tip constraints should be considered for probabilistic fracture-mechanics analysis. However, further studies involving other cracked structures and geometries are needed to evaluate this conclusion.

Acknowledgements

This work was supported by the Faculty Early Career Development Program of the US National Science Foundation (Grant no. CMS-9733058). The program directors were Drs Sunil Saigal and Ken Chong.

REFERENCES

1 R. H. Dodds, C. F. Shih and T. L. Anderson (1993) Continuum and micro-mechanics treatment of constraint in fracture. *Int. J. Fracture* **64,** 101–133.
2 C. Betegon and J. W. Hancock (1991) Two-parameter characterization of elastic–plastic crack fields. *J. Appl. Mech.* **58,** 104–113.
3 D. M. Parks (1992) Advances in characterization of elastic–plastic crack-tip fields. *Topics in Fracture and Fatigue*, Springer, New York, USA.
4 N. P. O'Dowd and C. F. Shih (1991) Family of crack-tip fields characterized by a triaxiality parameter: Part I—structure of fields. *J. Mech. Phys. Solids* **39,** 989–1015.
5 N. P. O'Dowd and C. F. Shih (1992) Family of crack-tip fields characterized by a triaxiality parameter: Part II—fracture applications. *J. Mech. Phys. Solids* **40,** 939–963.
6 S. Rahman (1995) A stochastic model for elastic–plastic fracture analysis of circumferential through-wall-cracked pipes subject to bending. *Engng Fracture Mech.* **52,** 265–288.
7 S. Rahman (1997) Probabilistic fracture analysis of pipes with circumferential flaws. *Int. J. Pressure Vessels Piping* **70,** 223–236.
8 S. Rahman and J. S. Kim (in press) Probabilistic fracture mechanics for nonlinear structures. *Int. J. Pressure Vessels Piping*.
9 S. Rahman (in press) Probabilistic fracture mechanics: *J*-estimation and finite element methods. *Engng Fracture Mech*.
10 J. R. Rice (1968) A path independent integral and the approximate analysis of strain concentration by notches and cracks. *J. Appl. Mech.* **35,** 379–386.
11 J. W. Hutchinson (1983) Fundamentals of the phenomenological theory of nonlinear fracture mechanics. *J. Appl. Mech.* **50,** 1042–1051 .
12 J. R. Rice and G. F. Rosengren (1968) Plane strain deformations near a crack tip in a power-law hardening material. *J. Mech. Phys. Solids* **16,** 1–12.
13 J. W. Hutchinson (1968) Singular behavior at the end of a tensile crack in a hardening material. *J. Mech. Phys. Solids* **16,** 13–31.
14 G. M. Wilkowski, F. Brust, R. Francini *et al.* (1991–94) Short cracks in piping and piping welds program. NUREG/CR-4599, 1–3 (1,2), US Nuclear Regulatory Commission, Washington, DC, USA.
15 A. M. Hasofer and N. C. Lind (1974) An exact and invariant first-order reliability format. *J. Engng Mech.* **100,** 111–121.
16 B. Fiessler, H. J. Neumann and R. Rackwitz (1979) Quadratic limit states in structural reliability. *J. Engng Mech.* **105**(EM4), 661–676.
17. R. Rackwitz and B. Fiessler (1978) Structural reliability under combined random load sequence. *Computers Structures* **9,** 484–494.
18. H. O. Madsen, S. Krenk and N. C. Lind (1986) *Methods of Structural Safety*, Prentice Hall, Englewood Cliffs, New Jersey, USA.
19 R. Y. Rubinstein (1981) *Simulation and the Monte Carlo Method*, John Wiley, New York, USA.
20 J. A. Joyce and R. E. Link (1997) Application of two parameter elastic–plastic fracture mechanics to analysis of structures. *Engng Fracture Mech.* **57,** 431–446.
21 ASTM Designation: E1737-96) (1996) Standard tests for J_{Ic} and determining *J–R* curves. American Society for Testing and Materials, West Conshohocken, Pennsylvania, USA.
22 Y. Murakami (1987) *Stress Intensity Factors Handbook*, Vols 1 and 2, 1st edition, Pergamon Press, New York, USA.
23 V. Kumar, M. D. German and C. F. Shih (1981) An engineering approach for elastic–plastic fracture analysis. EPRI NP-1931, Electric Power Research Institute, Palo Alto, California, USA.
24 A. S. Gullerud and R. H. Dodds (1995) *J–Q* and toughness scaling model solutions for M(T), DE(T), SE(T), SE(B) and C(T) specimens. UILU-ENG-95-2008, University of Illinois, Urbana, Illinois, USA.

APPENDIX A: *J*-INTEGRAL FOR SE(B) SPECIMENS

Consider a SE(B) specimen with span, S, width, W, thickness, B, crack length, a and load, P (see Fig. 4). If the deformation theory of plasticity is valid, the J-integral can be split as

$$J = J_e + J_p \tag{A1}$$

where J_e and J_p are the elastic and plastic components, respectively, of total J. They are described in the following subsections.

Elastic solution

Under plane-strain state of stress, the elastic J is[22,23]

$$J_e = \frac{K_I^2(1-\nu^2)}{E} \tag{A2}$$

where,

$$K_I = \frac{P}{B\sqrt{W}} \frac{3\dfrac{S}{W}\sqrt{a/W}}{2(1+2a/W)(1-a/W)^{3/2}} \times [1.99 - a/W(1-a/W) \times \{2.15 - 3.93a/W + 2.7(a/W)^2\}] \tag{A3}$$

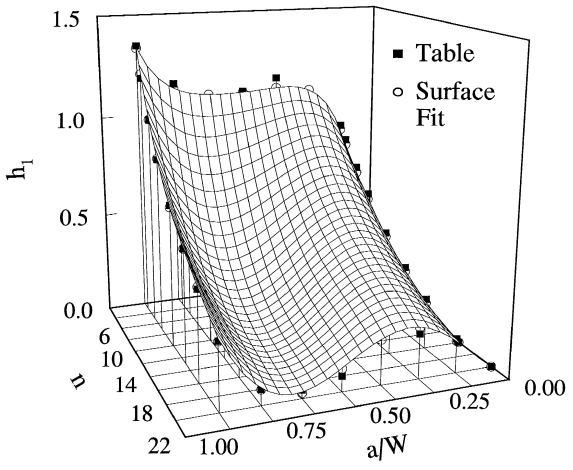

Fig. A1 Surface plot of $h_1(a/W, n)$.

is the mode-I stress-intensity factor, and ν is the Poisson's ratio.

Plastic solution

The plastic J can be calculated from[23]

$$\mathcal{J}_p = \frac{\alpha\sigma_0^2}{E}(W-a)h_1(a/W, n)\left(\frac{P}{P_0}\right)^{n+1} \tag{A4}$$

where

$$P_0 = \frac{1.455(W-a)^2 B\sigma_0}{S} \tag{A5}$$

is the reference load, and $h_1(a/W, n)$ is a dimensionless plastic influence function that depends on crack geometry and material hardening exponent. Assume that $h_1(a/W, n)$ can be expressed by

$$h_1(a/W, n) = \sum_{i=0}^{3}\sum_{j=1}^{5} D_{ij} n^i (a/W)^j \tag{A6}$$

where D_{ij}, $i = 0, 1, 2, 3$, and $j = 1, 2, 3, 4, 5$, are constant coefficients. Let $\boldsymbol{D} = [D_{ij}]$, $i = 0, 1, 2, 3$, and $j = 1, 2, 3, 4, 5$, be a 4×5 real matrix. Following least-squares analysis of $h_1(a/W, n)$ data calculated by finite element method[23] for various a/W and n, D can be estimated as

$$\boldsymbol{D} = \begin{bmatrix} 12.592 & -47.842 & 92.090 & -86.553 & 31.712 \\ -0.801 & 2.119 & -3.762 & 2.269 & 0.230 \\ -0.009 & 0.285 & -0.911 & 1.229 & -0.610 \\ 0.001 & -0.013 & 0.040 & -0.052 & 0.024 \end{bmatrix} \tag{A7}$$

Using Eq. (A6), Fig. A1 shows the surface plots of h_1 as a function of a/W and n. When compared with the tabulated values of Kumar *et al.*,[23] also shown in Fig. A1, the values of $h_1(a/W, n)$ calculated from Eq. (A6) are quite accurate. Hence, both the elastic and plastic components of $\mathcal{J}$ can be predicted analytically using Eqs (A2) and (A4), respectively.

APPENDIX B: *J–Q* ANALYSIS FOR SE(B) SPECIMENS

Consider a SE(B) specimen with its geometry, crack size and loads defined earlier. Assuming plane-strain condition and varying a/W, n and E/σ_0, Gullerud and Dodds[24] conducted extensive non-linear finite element analysis to generate $\mathcal{J}$–Q results. This suggests that for simple structures, e.g. SE(B), response surface equations can be developed correlating Q with $\mathcal{J}$. For a fixed E/σ_0, consider the following approximation of Q, given by

$$Q\left(\mathcal{J}/\min(a, b)\sigma_0, a/W, n\right) = \sum_{i=0}^{3}\sum_{j=1}^{3} E_{ij}(n)(a/W)^i \left(\mathcal{J}/\min(a, b)\sigma_0\right)^j \tag{B1}$$

where, $b = W - a$, and

$$E_{ij}(n) = F_{ij} + G_{ij} n + H_{ij} n^2 \tag{B2}$$

with F_{ij}, G_{ij} and H_{ij}, $i = 0, 1, 2, 3$; and $j = 1, 2, 3$, are coefficients that may depend only on E/σ_0. Let $\boldsymbol{F} = [F_{ij}]$, $\boldsymbol{G} = [G_{ij}]$ and $\boldsymbol{H} = [H_{ij}]$, $i = 0, 1, 2, 3$; and $j = 1, 2, 3$, be 4×3 real matrices. Following regression analysis of $\mathcal{J}$–Q results for $E/\sigma_0 = 500$,[24] it was determined that,

$$\boldsymbol{F} = \begin{bmatrix} -26.35 & -2578.81 & 121\,245 \\ -297.63 & 62\,155.60 & -2\,101\,770 \\ 1665.14 & -251\,662.00 & 7\,941\,150 \\ -1663.03 & 239\,361.00 & -7\,431\,860 \end{bmatrix} \tag{B3}$$

$$\boldsymbol{G} = \begin{bmatrix} -6.69 & 432.16 & -12\,720.90 \\ 53.39 & -5889.46 & 196\,497.00 \\ -203.17 & 24\,868.90 & -795\,823.00 \\ 202.16 & -25\,376.70 & 791\,575.00 \end{bmatrix} \tag{B4}$$

and

$$\boldsymbol{H} = \begin{bmatrix} 0.23 & -16.23 & 511.42 \\ -1.84 & 230.53 & -8082.77 \\ 7.89 & -1030.58 & 33\,684.10 \\ -8.33 & 1084.07 & -34\,116.90 \end{bmatrix} \tag{B5}$$

Figure B1 shows the plots of Q from Eq. (B1) (lines) as a function of $\mathcal{J}/\min(a, b)\sigma_0$ and a/W, for $n = 5$, 10 and 15. Also plotted in the same figure are the corresponding finite element results (points) of Gullerud and Dodds.[24] The agreement between these two sets of results is excellent. Hence, Eq. (B1) can be used to calculate Q for $E/\sigma_0 = 500$, when $\mathcal{J}$, a/W and n are prescribed.

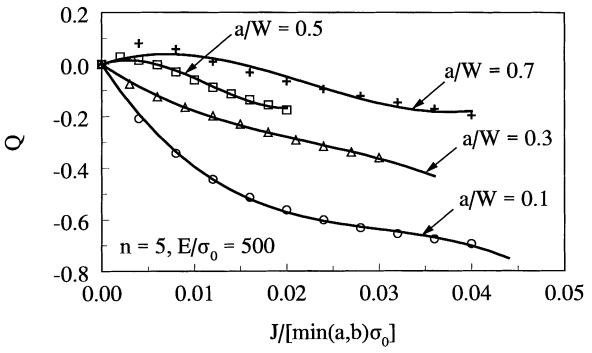

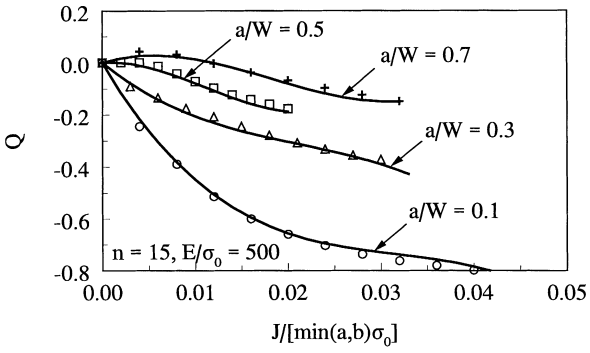

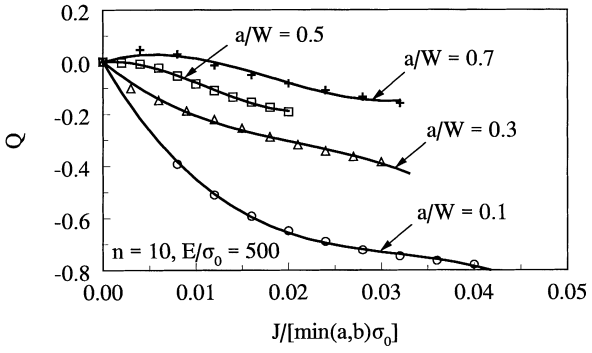

Fig. B1 Plots of Q for $n = 5$, 10 and 15.